IOP Publishing and International Atomic Energy Agency Nuclear Fusion
Nucl. Fusion **49** (2009) 075015 (8pp) doi:10.1088/0029-5515/49/7/075015

Spectral effects on fast wave core heating and current drive

C.K. Phillips[1], R.E. Bell[1], L.A. Berry[2], P.T. Bonoli[3], R.W. Harvey[4], J.C. Hosea[1], E.F. Jaeger[2], B.P. LeBlanc[1], P.M. Ryan[2], G. Taylor[1], E.J. Valeo[1], J.B. Wilgen[2], J.R. Wilson[1], J.C. Wright[3], H. Yuh[5] and the NSTX Team

[1] PPPL, Princeton University, Princeton, NJ 08540, USA
[2] ORNL, Oak Ridge, TN 37831, USA
[3] PSFC, MIT, Cambridge, MA 02139, USA
[4] CompX, Del Mar, CA 92014, USA
[5] Nova Photonics, Princeton, NJ 08540, USA

E-mail: ckphillips@pppl.gov

Received 31 December 2008, accepted for publication 29 April 2009
Published 4 June 2009
Online at stacks.iop.org/NF/49/075015

Abstract
Recent results obtained with high harmonic fast wave (HHFW) heating and current drive (CD) on NSTX strongly support the hypothesis that the onset of perpendicular fast wave propagation right at or very near the launcher is a primary cause for a reduction in core heating efficiency at long wavelengths that is also observed in ICRF heating experiments in numerous tokamaks. A dramatic increase in core heating efficiency was first achieved in NSTX L-mode helium majority plasmas when the onset for perpendicular wave propagation was moved away from the antenna and nearby vessel structures. Efficient core heating in deuterium majority L-mode and H-mode discharges, in which the edge density is typically higher than in comparable helium majority plasmas, was then accomplished by reducing the edge density in front of the launcher with lithium conditioning and avoiding operational points prone to instabilities. These results indicate that careful tailoring of the edge density profiles in ITER should be considered to limit radio frequency (rf) power losses to the antenna and plasma facing materials. Finally, in plasmas with reduced rf power losses in the edge regions, the first direct measurements of HHFW CD were obtained with the motional Stark effect (MSE) diagnostic. The location and radial dependence of HHFW CD measured by MSE are in reasonable agreement with predictions from both full wave and ray tracing simulations.

PACS numbers: 52.50.Qt, 52.55.Fa, 52.35.Hr

1. Introduction

Radio frequency (rf) heating and current drive (CD) are essential components in many magnetic fusion devices, including ITER. Experimental and theoretical studies on NSTX are focused on optimizing core heating and CD efficiency by minimizing power losses in the edge regions, an issue of importance in ITER [1]. These studies are also needed to establish the viability of devices based on the spherical torus (ST) concept, such as ST-CTF [2], which may depend on rf waves to sustain long-pulse reactor-grade plasmas and assist with noninductive plasma start-up. In the NSTX device, the effectiveness of high harmonic fast waves (HHFW) for providing core heating and $q(0)$ control to establish fully noninductively sustained H-mode scenarios, and for providing HHFW-driven bootstrap current for noninductive CD during the ramp-up phase of the discharge, is under investigation.

The HHFW system on NSTX is particularly well suited for studying the competition between core heating and edge power losses as a function of antenna phasing. The NSTX HHFW launcher has 12 antenna straps that can deliver up to 6 MW at 30 MHz [3]. By feeding this strap array with six decoupled sources, very good toroidal spectral definition is obtained. In NSTX, the equilibrium magnetic field lines in front of the launcher have a significant pitch with respect to the vertically aligned antenna straps, by virtue of the larger edge poloidal field components in an ST device relative to a conventional tokamak. Hence, there is a significant difference in the launched parallel wave spectrum relative to the toroidal spectrum that depends on the safety factor, q, at the edge. Figure 1 shows the relative power coupled into the plasma as a

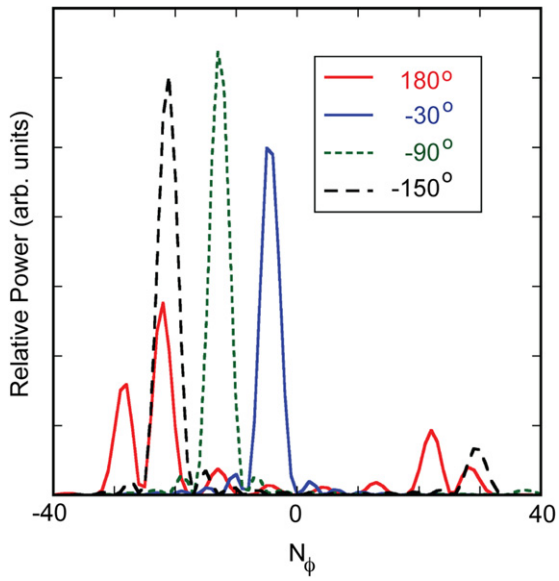

Figure 1. NSTX antenna spectrum (power coupled into plasma) versus N_ϕ for different phasings.

function of the toroidal mode number, N_ϕ, for various set strap-to-strap phasings, ranging from -30° to $+180^\circ$, calculated with the RANT3D code for plasma conditions typical of those discussed in this paper [3].

Because of the inherently high beta of NSTX plasmas, the HHFWs experience strong nearly single pass absorption via electron Landau damping and transit time magnetic pumping [4]. Shown in figure 2 are ray paths in the toroidal cross sections in (*a*) and (*c*) and the poloidal cross sections in (*b*) and (*d*), obtained with the GENRAY code [5, 6] for waves launched with parallel wave numbers, $k_\parallel$, over the range accessible with the 12-strap antenna for typical OH target conditions ($n_{e0} = 3.3 \times 10^{19}$ m^{-3}, $T_{eo} = 1.1$ keV) in (*a*) and (*b*), and for the rf-heated plasma conditions (slightly hollow density profile, $n_{e0} = 2.3 \times 10^{19}$ m^{-3}, peak $n_e = 2.7 \times 10^{19}$ at $\rho \sim 0.3$, $T_{eo} = 2.8$ keV) in (*c*) and (*d*). The solid dot at the end of each ray path represents the point at which at least 80% of the power launched on that ray has been absorbed. As expected from theory [4, 7], the absorption rate increases as the plasma is heated and is lower for the ray launched with -30° phasing. However, it is interesting to note that even this ray is strongly absorbed in less than a single toroidal or poloidal transit of the rf-heated plasmas. The interaction of these waves with the inner wall of the vessel is also minimal, due to the $n_\parallel^2 = R$ cutoff [7] that moves significantly into the plasma on the high field side of the magnetic axis. These absorption properties of the HHFWs in NSTX provide the opportunity to study core heating as a function of antenna phasing and to separate out rf power losses near the antenna from rf power losses elsewhere in the plasma.

In this paper, experimental studies on NSTX of the dependence of the core heating and CD efficiency as a function of the antenna phasing are discussed and compared with simulations obtained with a range of advanced state-of-the-art rf simulations. The results of these studies strongly support the hypothesis that the onset of fast wave propagation right at or very near the launcher is a primary cause of the reduced core heating efficiency observed at long wavelengths [8] in NSTX and in ICRF heating experiments in numerous tokamaks. Perpendicular wave propagation begins when the local edge electron density exceeds the critical electron density, n_{ec}, at the $n_\parallel^2 = R$ cutoff of the fast wave. In the HHFW frequency range, in which the wave frequency is much higher than the local fundamental ion cyclotron frequencies and much lower than the local lower hybrid frequency, the cutoff condition is given approximately by $n_\parallel^2 \approx \omega_{pe}^2/(\omega^*|\Omega e|)$, when the density is sufficiently high so that the contributions of the displacement current can be ignored. Hence, the critical density is proportional to $k_\parallel^2 \times B/\omega$. A dramatic increase in core heating efficiency was achieved in NSTX L-mode helium-4 majority plasmas when the edge density was lowered, thereby moving the location where the HHFWs start to propagate away from the antenna and nearby vessel structures. The heating efficiency scales with the launched antenna spectrum and the local magnetic field, consistent with the scaling of the critical density for onset of perpendicular wave propagation [8]. These results indicate that careful balancing of the edge density in front of the antenna in ITER may be required to limit edge power losses from direct fast wave damping while at the same time ensuring adequate coupling of the power into the plasma. Finally, the location and radial profile of HHFW CD measured with the motional Stark effect (MSE) diagnostic [9], obtained in plasmas with reduced rf power losses in the edge, are discussed. The measurements are in reasonable agreement with simulations obtained from the GENRAY ray tracing code, as well as the AORSA [10] and TORIC [11] full wave codes.

2. Fast wave core heating efficiencies in NSTX

The core heating efficiency in NSTX in L-mode plasmas composed primarily of helium-4 has been inferred from a series of similar discharges at fixed phasing but different magnetic field strengths, and at fixed magnetic field with a range of phasings. In order to quantify the amount of rf power deposited in the core of the plasma, rf power pulses are applied and the time evolution of either the electron stored energy, W_e, or the total stored energy, W_T, is fitted with an exponential rise function of the form

$$W(t) = W_0 - (W_0 - W_F) \times (1 - e^{-t/\tau_e}), \qquad (1)$$

where W_0 is the relevant stored energy at the beginning of the pulse and W_F is the asymptotic value that would have been obtained in the steady-state limit [12]. The electron stored energy is evaluated by integrating the kinetic electron pressure measured by Thomson scattering over the magnetic field surface volumes inferred from the magnetic equilibrium code, EFIT [13]. The rf-induced change in the electron stored energy, ΔW_e, is equal to the difference between W_F and the asymptotic value of W_e that would have been obtained without the rf pulse, while the rf power into electrons in the core is given by $P_{rf,e} = \Delta W_e/\tau_e$. Finally, the core electron heating efficiency is then defined by $\eta_e = P_{rf,e}/\Delta P_{rf}$, where ΔP_{rf} is the increment in the applied rf power in the pulse. For the experiments described in this report, the change in the ohmic heating power during the rf pulse is less than 100 kW, as inferred from changes in the loop voltage and plasma current,

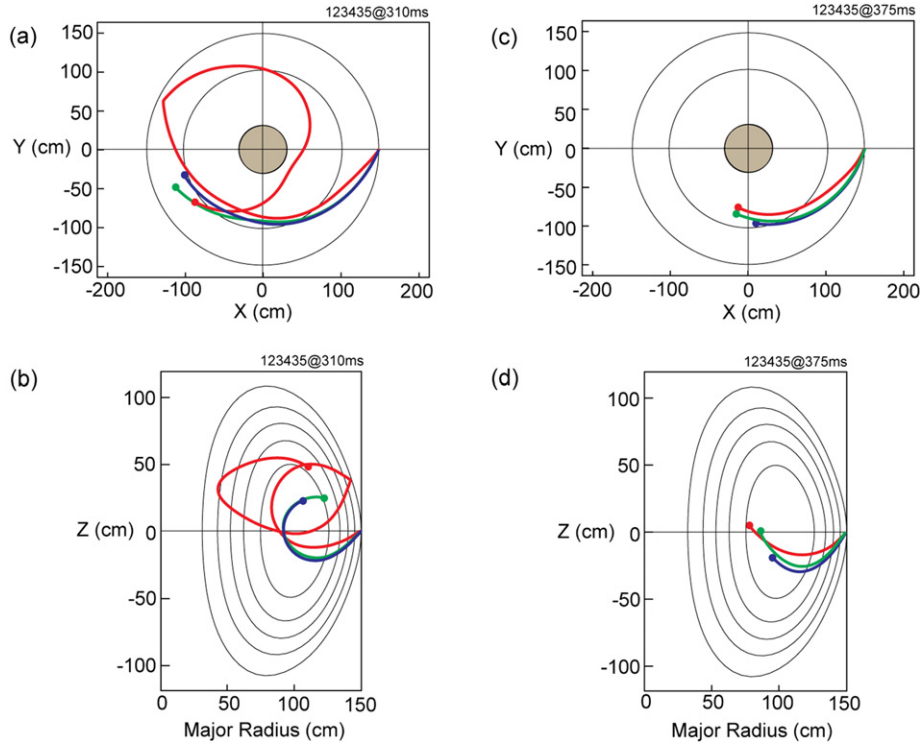

Figure 2. Ray paths for -30° (red), -90° (blue) and 180° (green) strap-to-strap antenna phasings for OH target conditions ((*a*) toroidal, (*b*) poloidal views) and for rf-heated plasma conditions ((*c*) toroidal, (*d*) poloidal views), for a discharge with $B_{T0} = 0.55$ T and $I_p = 600$ kA. The solid dot shows where 80% of initial power is absorbed.

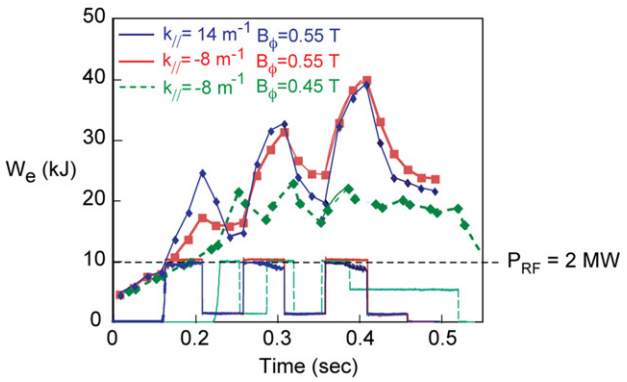

Figure 3. Time evolution of the electron stored energy during rf heating at different B_T for fixed phasing, and for different phasing at fixed B_T.

and so can be neglected in the core heating efficiency estimates. The total core heating efficiency, η_T, is similarly inferred using the time evolution of total stored energy, W_T, obtained from EFIT. For the plasma conditions obtained in these experiments, the HHFWs are predicted to damp directly almost entirely on the electrons [4], so changes in W_e are a reasonable measure of the HHFW power deposition to the bulk of the plasma [8, 12].

In previous experiments [12] at a fixed toroidal magnetic field of 0.45 T, a plasma current of 0.6 MA, line-integrated electron densities of $n_{el} \sim 2.5 \times 10^{19}\,\mathrm{m}^{-2}$, and otherwise similar plasma conditions, the core electron heating efficiency for a fixed strap-to-strap phasing of -90° ($k_\parallel = -8\,\mathrm{m}^{-1}$) was approximately equal to 22%, in contrast to the 48% efficiency achieved with 180° phasing ($k_\parallel = 14\,\mathrm{m}^{-1}$). The corresponding total core heating efficiencies at these phasings were 44% and 68%, respectively [8, 12]. Power losses due to parametric decay instabilities (PDIs) and associated edge ion heating were comparable for both of these phasings, and hence could not account for the large difference in core heating efficiencies [8]. These experiments were later repeated at a higher magnetic field of 0.55 T, with a plasma current of 0.72 MA, chosen to keep the edge q approximately the same as in the experiments at 0.45 T. Similar densities were achieved at the higher B_T, ranging from $n_{el} \sim 2 \times 10^{19}\,\mathrm{m}^{-2}$ during the first rf pulse to $\sim 2.5 \times 10^{19}\,\mathrm{m}^{-2}$ during the second and third rf pulses. The results are shown for ΔW_e in figure 3 and for ΔW_T in figure 6 later on. As seen in figure 3, the change in ΔW_e is about a factor of 2 higher at $B_\phi = 0.55$ T than at 0.45 T for -90° phasing ($k_\parallel = -8\,\mathrm{m}^{-1}$). Note moreover that with the magnetic field fixed at 0.55 T, comparable increments in ΔW_e were obtained at both -90° and 180° phasings for the second and third rf pulses in the discharges, but not in the first pulse, where the observed increase in ΔW_e is noticeably less with the -90° phasing ($k_\parallel = -8\,\mathrm{m}^{-1}$). During the first rf pulse for the shots at 0.55 T, the edge density measured approximately 2 cm in front of the antenna with the Thomson scattering diagnostic exceeded the critical density of $5 \times 10^{17}\,\mathrm{m}^{-3}$ for onset of wave propagation perpendicular to the magnetic field at $k_\parallel = -8\,\mathrm{m}^{-1}$, but not during the second and third pulses, when the heating efficiency for both the $k_\parallel = -8\,\mathrm{m}^{-1}$ and $14\,\mathrm{m}^{-1}$ cases is comparable. During the second and third pulses at 0.55 T, the time-averaged ratio of the electron density, measured 2 cm in front of the antenna, relative to the critical density, $\langle n_e/n_{ec}\rangle$, is equal to 0.81 ± 0.12 with the -90° phasing and 0.24 ± 0.05 with the 180° phasing.

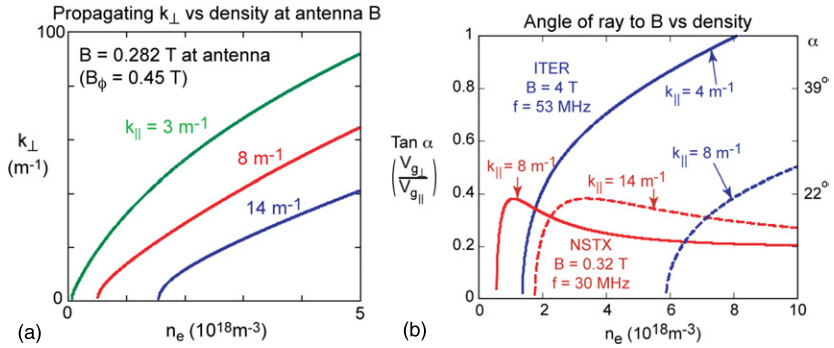

Figure 4. Dispersion relation (*a*) and angle of group velocity (*b*) with respect to magnetic field show that lower phasings propagate closer to the wall for a given density profile.

For these two discharges, the distance between the last closed flux surface and the Faraday shield surface was approximately 4.4 cm. For the earlier discharge taken at 0.45 T with -90° phasing, the ratio $\langle n_e/n_{ec}\rangle$, also time-averaged over the second and third rf pulses, was approximately equal to 1.02 ± 0.3, with $n_{ec} \sim 4 \times 10^{17}\,\mathrm{m}^{-3}$. This higher ratio is consistent with the observed reduced change in W_e at the lower B_T. For this discharge, the distance between the last closed flux surface and the antenna straps was approximately 5.3 cm, suggesting that significant wave propagation occurs outside of the last closed flux surface in the vicinity of the launcher and surrounding vessel structures. However, because the energy confinement tends to improve while the edge density profiles tend to be steeper at higher B_T, it is more difficult to separate out the effects of antenna phasing, onset of wave propagation and improved confinement when comparing discharges at 0.45 T to those at 0.55 T. During these experiments, the edge reflectometer was used to measure the edge density profile on some shots and PDIs on others, with the result that edge density profiles are not available on enough of the discharges to quantify the separation distance between the antenna face and the location where perpendicular wave propagation begins, as a function of magnetic field and antenna phasing. These studies will be conducted in future experimental campaigns on NSTX. Nevertheless, the correlation reported here between the change in W_e and the ratio $\langle n_e/n_{ec}\rangle$ at 2 cm in front of the antenna, as a function of antenna phase, strongly suggests that onset of wave propagation near the antenna or vessel wall can lead to a substantial decrease in core heating efficiency and corresponding loss of power in the edge regions.

The propagation of HHFWs can be reasonably simulated using a cold plasma model [4]. In figure 4(*a*), the cold plasma wave propagation characteristics for the HHFWs are displayed as a function of the edge density for a magnetic field strength of 0.282 T in front of the antenna, corresponding to the 0.45 T on axis case shown in figure 3. For a given $k_\parallel$, if the edge density is too low, the wave is 'cut off' ($k_\perp = 0$) and does not propagate into the plasma. In this case, the wave will 'evanesce' into the plasma until it reaches a point where the local density exceeds the critical density and propagation commences. The local group velocity then specifies the direction in which the wave energy subsequently propagates in to the plasma. In figure 4(*b*), the angle that the group velocity makes with respect to the edge magnetic field is drawn for HHFW heating (180°) and CD phasings (90°) in NSTX as well as for low harmonic ICRF heating and CD in ITER. The HHFWs in NSTX tend to propagate at a small angle relative to the equilibrium magnetic field over the range of operating densities, while the lower harmonic fast waves in ITER can penetrate more readily across the field lines as the density encountered by the waves increases.

As inferred from figure 4(*a*), for a given edge density profile and magnetic field, the waves with the lower launched $k_\parallel$'s begin to propagate much closer to the antenna than those with higher $k_\parallel$'s. Increasing the edge magnetic field moves the onset for propagation away from the antenna for all values of $k_\parallel$, for a fixed frequency. If the waves begin to propagate too close to the antenna, the NSTX results presented here suggest that power is lost in the edge regions, most likely due to such processes as collisions, rf sheaths, and sputtering associated with direct fast wave interactions in the vicinity of the antenna and surrounding structures. Previous studies of ICRF heating at lower harmonics indicate that if the distance between the antenna and the point at which propagation begins is too large, that it becomes difficult to couple sufficient power into the plasma. For this reason, the ITER project is considering enhancing the scrape-off density to improve coupling with a large antenna–plasma gap [1, 14]. Since the density profile in the scrape-off region of ITER is presumed to be rather flat, if the density near the launcher is close to and slightly above the critical density, then the ICRF waves may propagate for a considerable distance at a relatively small angle relative to the equilibrium field, until the local density finally increases. Thus it is possible that wave propagation will occur near the blanket surface and the antenna in ITER under these conditions. The NSTX results indicate that careful balancing of the edge density in front of the antenna in ITER may be required to limit edge power losses from direct fast wave damping while at the same time ensuring adequate coupling of the power into the plasma.

Though the results presented here indicate that the onset of perpendicular wave propagation near the launcher correlates with the observed degradation of core heating efficiency at the smaller launched $k_\parallel$'s, further studies are needed to identify the specific edge loss mechanisms responsible for the degradation. As mentioned previously, this trend is also observed in low harmonic ICRF heating in conventional tokamaks, where the core heating efficiency with 180° phasing is always substantially higher than that obtained with 0° phasing [15]. A number of mechanisms have been proposed,

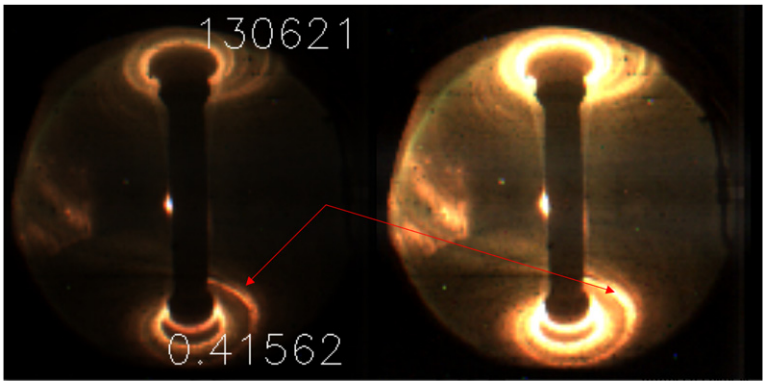

Figure 5. Visible light camera picture showing toroidally localized HHFW interaction with the divertor in an NSTX H-mode plasma ($I_p = 1$ MA, $P_{NB} = 2$ MW, $B_T = 0.55$ T, $P_{rf} \sim 1.8$ MW, $-90°$ phasing). Different exposure times were used for the two frames in the figure.

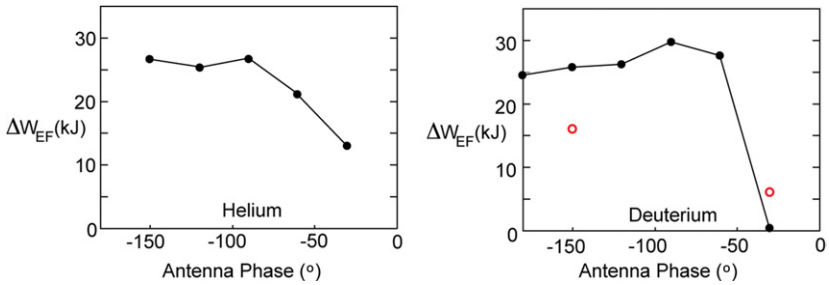

Figure 6. Rf-induced increments in electron stored energy comparable in both He-4 ($P_{rf} \sim 1.8$ MW, 80 ms pulse) and D ($P_{rf} \sim 1.1$ MW, 230 ms pulse) discharges. Open circles (red) indicate results obtained with shorter rf pulses ($P_{rf} \sim 1.3$ MW, 67 ms pulse) in D discharges with Li injection.

including collisional losses [15], surface wave propagation associated with large poloidal wave numbers excited by sharp boundaries of the current strap in the poloidal direction [15], antenna reactive field losses [8] and rf sheath dissipation [16–18]. The power losses from most of these mechanisms are predicted to increase at higher edge densities. The collisional losses in the edge are predicted to decrease at higher antenna phasings [15]. PDIs may account for some of the losses, but as discussed above, are not large enough to account for the observed degradation of the core heating efficiency on NSTX, so that a number of processes may be contributing to the net loss. Sheath rectification losses in particular are associated with hot spots on antennas and nearby limiters and in general are exacerbated when the current straps are not aligned with the equilibrium magnetic field [16–18]. Visible light pictures, taken with a fast camera at the end of the 2008 experimental campaign, of a few NSTX H-mode discharges with and without HHFW heating, provide evidence that fast wave interactions in the scrape-off-layer appear to be heating tiles on the outside of the divertor in the bottom of the vessel. As shown in figure 5, the toroidally localized hot spot appears to be linked with the antenna along the field lines and is absent in discharges without HHFW heating. Note that the slant of the equilibrium magnetic field lines relative to the vertically oriented antenna straps is particularly evident on the left-hand side of the discharge. It is not clear if the heating is due to direct interaction of the waves with the divertor surface, or from the impact of particles accelerated by the rf along the magnetic field lines, or if sheath effects are responsible. Based on the few visible light pictures available, the intensity of the hot spot appears to be more intense with lower antenna phasings, and to decay away on time scales consistent with conductive and/or radiative cooling when the HHFW is turned off. More detailed studies of the dependence of the hot spot and its time evolution on the HHFW power, antenna spectrum, edge densities, and ELM behaviour are planned for the upcoming run campaign on NSTX and will be reported in a future paper.

Previous HHFW heating experiments on NSTX in deuterium plasmas at 0.45 T were rather unsuccessful [8], in part because control of the density is more difficult in deuterium than in helium operation, so the edge densities tended to be higher. After extensive wall conditioning and avoidance of MHD activity that in general can degrade the overall confinement and stability and time evolution of a discharge, HHFW heating in deuterium plasmas at the higher magnetic field of 0.55 T was as successful as that in helium plasmas [3], as seen in figure 6. Indeed, central electron temperatures of 5 keV have now been achieved in both He and D plasmas at $B_T = 0.55$ T with the application of 3.1 MW HHFW at $-150°$ antenna phasing [19]. The rf induced change in total stored energy still dropped precipitously below $-60°$ phasing for this initial phase scan in deuterium. According to the Thomson scattering diagnostic, the edge density for the $-30°$ discharge was significantly higher than in the other discharges in the scan, most likely due to an MHD instability whose presence correlated with the time evolution of the edge density. Measurements indicate the edge density 2 cm in front of the antenna for the $-30°$ discharge was approximately 1.8×10^{18} m^{-3}. This density is above the critical density for propagation consistent with the conclusion that

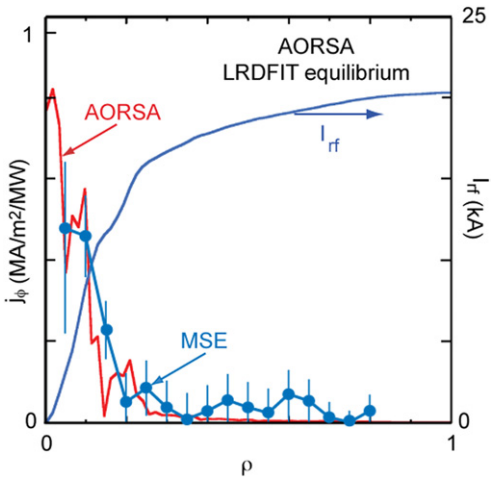

Figure 7. Comparison of MSE data with AORSA full spectrum simulation using MSE-constrained equilibrium obtained with LRDFIT.

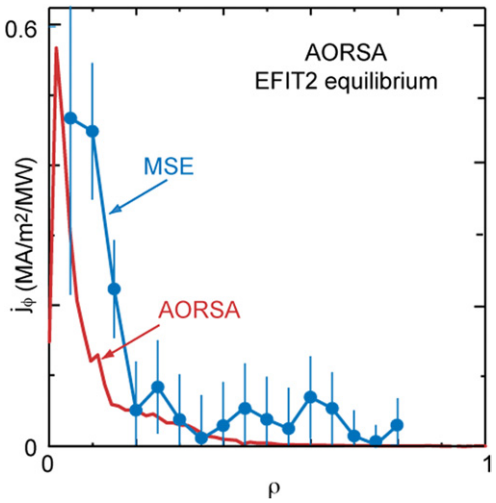

Figure 8. Comparison of MSE data with AORSA full spectrum simulation using an equilibrium fit, without the MSE constraint, from EFIT2.

high edge densities lead to increased edge power losses and corresponding degradation of the core heating efficiency. With additional edge conditioning obtained with lithium injection, a further reduction in the edge density at -30° phasing to 0.5×10^{18} m^{-3} was observed with the edge reflectometer [20], resulting in the first significant heating in D plasmas at this phasing, as indicated by the open circle (red) at -30° in figure 6. However, the rf pulse length in the discharges with Li conditioning were only about 67 ms in duration, compared with the 230 ms duration for the scan of deuterium discharges shown in figure 6. As a result, the stored energy increment obtained at -150° phasing in the discharges with the Li conditioning was less than in the longer discharges without it. Because of this difference in rf pulse lengths, it is difficult to accurately compare the performance of the discharges. Nevertheless, these studies indicate that extensive conditioning to reduce the edge density results in better core heating efficiencies over a range of antenna phasings, consistent with the conclusion that edge power losses can be significant if the wave begin to propagate too close to the launcher and surrounding structures.

3. MSE measurements of HHFW CD

By operating at higher magnetic fields and with reduced edge densities, the first direct measurements of HHFW co-CD [8] at an antenna phasing of -90° were obtained with the MSE diagnostic [9]. The MSE measurements, obtained using modest rf power (~1.8 MW) and short rf pulses (~80 ms), indicate that about 15 kA of noninductive current was driven by the HHFWs within $\rho \leqslant 0.2$, as shown in figure 7. The magnitude of the driven current profile is normalized assuming that 67% of the launched power, or about 1.2 MW of power, is actually coupled into the core plasma, consistent with changes in the total stored energy of the discharge. Even with the modest power and rf pulse lengths used so far, the rf-driven current is sufficient to transiently decrease $q(0)$ from 1.0 to 0.6, as inferred from the pitch angles near the axis measured by the MSE diagnostic. Simulations obtained with the AORSA code [10], using the Ehst–Karney (E–K) parameterization [21] and the full spectrum of launched waves, are shown in figure 7

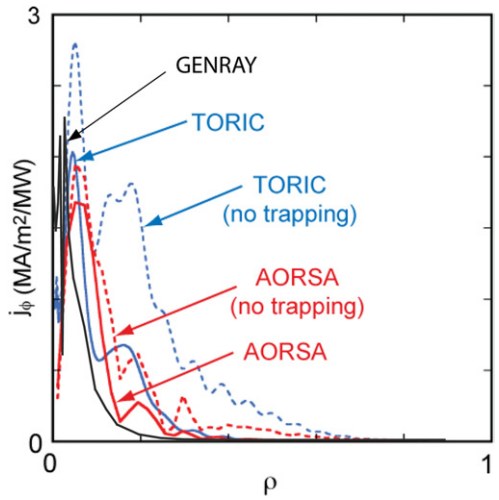

Figure 9. AORSA and TORIC simulations, with and without trapping, and GENRAY, with trapping, of the HHFW-CD for $N_\phi = 12$.

for comparison. Electron trapping effects effectively limit the rf-driven current to the plasma core in NSTX and other ST devices, consistent with the MSE measurements and previous modelling studies [22]. It is important to note that agreement between the simulations and the measurements improves as the plasma parameters used in the equilibrium reconstructions are more tightly constrained by experimental measurements. In particular, better agreement is found by using an equilibrium fit constrained by the actual MSE pitch angle measurements and kinetic plasma profiles, as shown in figure 7 with the LRDFIT [23] code, rather than the equilibrium fit constructed without the MSE constraint, as shown in figure 8 from EFIT2.

Simulations of the noninductive driven current in this discharge obtained with the AORSA and TORIC full-wave codes, using the E–K parameterization, as well as the GENRAY/CQL3D ray tracing and bounce-averaged Fokker–Planck package, are remarkably consistent, as shown in figure 9. The noninductive driven current density profiles are shown for the single peak toroidal mode number, $N_\phi = 12$,

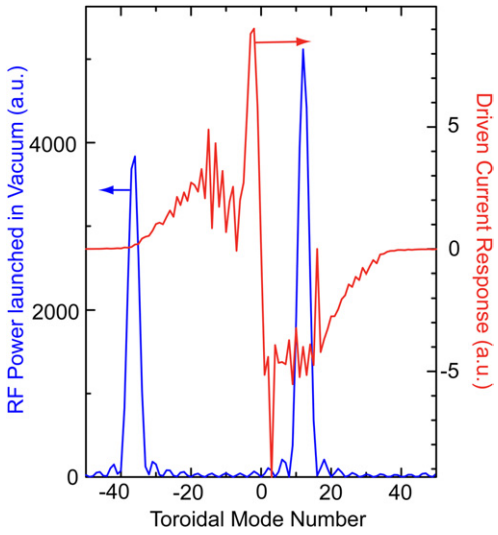

Figure 10. RF power launched in vacuum and corresponding driven current response, from the AORSA code.

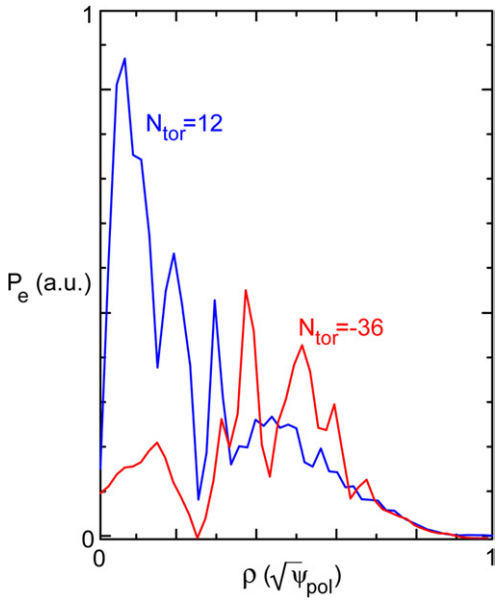

Figure 11. Radial power deposition profiles from AORSA for $N_{\rm tor} = 12$ and $N_{\rm tor} = -36$, showing off-axis deposition at the higher toroidal mode number.

launched by the HHFW antenna. Note that the predicted magnitude of the noninductive currents obtained with $N_\phi = 12$ is considerably higher than that obtained with the full spectrum that is shown in figure 7, indicating the importance of including the back lobes of the spectrum in the simulations. The driven current response as a function of the toroidal mode numbers retained in the full spectrum, obtained with AORSA and including trapping effects for each N_ϕ, is compared with the vacuum spectrum launched by the antenna for -90° in figure 10, while the corresponding radial power deposition profiles for the vacuum spectra peaks at $N_\phi = 12$ and $N_\phi = -36$ are shown in figure 11. These simulations indicate that the power on the back lobe, which is launched at a very high $k_\parallel (N_\phi \sim -38)$, is damped well off-axis, where the corresponding noninductive driven current is lost due to trapping effects. This effectively reduces the power available for CD by about 50%, thereby accounting for the difference in magnitude between the integrated currents found with the full spectrum in figure 7 and the single N_ϕ spectrum in figure 9.

The GENRAY/CQL3D simulation, with a single N_ϕ, for this particular discharge, indicates that the driven current profile may be somewhat narrower than suggested by the E–K parameterization. Since the E–K parameterization is based on solutions of the adjoint equation for rf-driven currents in conventional aspect ratio tokamaks, the difference may be due to the more accurate treatment of the NSTX equilibrium in the calculation of the driven current in CQL3D, but further comparisons to more accurate experimental measurements will be needed to quantify this effect. Simulations with the GENRAY code, which can solve for the induced current using the ADJ module [24] instead of CQL3D to solve the adjoint equation for the exact NSTX equilibrium are also underway and will be compared in the future with the MSE data and the full-wave simulations provided here. As these wave modules are integrated into the TRANSP transport analysis code [25], further simulation studies will be able to examine the impact of neglecting the back EMF on the driven current profile (the assumption of steady-state conditions).

4. Conclusions

The results obtained with HHFW heating and CD on NSTX strongly support the hypothesis that the onset of fast wave propagation right at or very near the launcher is a primary cause for the reduced core heating efficiency observed at long wavelengths [8] in ICRF heating experiments in numerous tokamaks. Since the critical density needed for wave propagation scales as $B \times k_\parallel^2/\omega$ [7], moving the location at which the fast waves begin to propagate away from the antenna and nearby structures, by increasing the magnetic field and extensive conditioning to reduce the edge density, resulted in better core heating efficiencies over a range of antenna phasings. The observed degradation at the lowest antenna phasing is thus most likely due to power losses from collisions, rf sheaths and sputtering associated with direct fast wave interactions in the vicinity of the antenna and surrounding structures. The impact of these various loss mechanisms on lower harmonic ICRF heating in conventional aspect ratio tokamaks has been discussed in previous studies [15–18]. The impact is particularly pronounced in NSTX since the HHFWs are nearly totally damped in a single transit of the device. It is thus likely that the main power losses to the edge occur from the initial interactions with the antenna and surrounding structures. This makes the NSTX plasma an ideal test-bed for benchmarking models in advanced RF codes for RF power loss in the vicinity of the antenna. Numerical studies to evaluate the relative importance of these various edge loss mechanisms are underway in the RF SciDAC project [26]. The ITER project is considering enhancing the scrape-off density to improve coupling with a large antenna–plasma gap [1, 14]. The NSTX results indicate that careful balancing of the edge density in ITER should be considered to limit edge power losses from direct fast wave interactions with the antenna and plasma facing materials while at the same time ensuring adequate coupling of power across the evanescent layer in front of the launcher.

Experiments have begun on NSTX to optimize HHFW core heating of neutral beam driven H-mode deuterium plasmas. Again with a well conditioned wall, significant core electron heating, as evidenced by an increase of ~0.7 keV in $T_e(0)$ and a factor of ~2 in central electron pressure, has been observed for 0.55 T operation with an antenna phase of 180° ($k_\parallel = \pm 14\,\mathrm{m}^{-1}$, $18\,\mathrm{m}^{-1}$) [19]. This result contrasts strongly with the total lack of heating found earlier at $B_T = 0.45$ T in deuterium plasmas, and is useful for the study of electron transport in the NSTX core plasma [27]. Over the next few years, NSTX experiments will explore HHFW CD in L- and H-mode deuterium plasmas with longer rf pulses and higher rf power to permit more accurate and nearer steady-state MSE measurements. Simulations obtained thus far with the AORSA and TORIC full-wave codes, using the E–K parameterization, as well as the GENRAY/CQL3D ray tracing and bounce-averaged Fokker–Planck package, are remarkably consistent with MSE measurements of approximately 15 kA of noninductive driven current within $\rho \leqslant 0.2$ for 1.8 MW of input rf power (~1.2 MW absorbed). The comparisons highlight the impact of trapping effects on noninductive currents driven off-axis and indicate the need to optimize the launched spectrum to minimize trapping-related degradation in the CD efficiency. However, even with the modest power and rf pulse lengths used so far, the rf-driven current is sufficient to transiently decrease $q(0)$ from 1.0 to 0.6, as inferred from the pitch angles near the axis measured by the MSE diagnostic. With the ability to drive both co and counter CD by appropriate phasing between the launcher straps, the HHFW system may therefore provide a tool for $q(0)$ control, needed to achieve long pulse high performance discharges in NSTX and future ST and other fusion devices.

Acknowledgments

The authors wish to acknowledge the support of Dr Masayuki Ono and Dr Jonathan Menard, the NSTX team and the machine, RF, and neutral beam operations groups.

This work was supported by USDOE Contract No. DE-AC02-76CH03073.

References

[1] Swain, D.W. and Goulding R.H. 2007 *Fusion Eng. Des.* **82** 603–9
[2] Peng Y.-K. M. *et al* 2005 *Plasma Phys. Control. Fusion* **47** B263
[3] Ryan P.M. *et al* 2008 *35th EPS Conf. on Plasma Physics (Hersonissos, Crete, Greece, June 2008)* paper P1.108 http://epsppd.epfl.ch/Hersonissos/pdf/P1_108.pdf
[4] Ono M. 1995 *Phys. Plasmas* **2** 4075–82
[5] Smirnov A.P. and Harvey R.W. 1995 *Bull. Am. Phys. Soc.* **48** 1837
[6] Smirnov A.P. and Harvey R.W. 2003 The GENRAY Ray Tracing Code *Report CompX-2000-01* Version 2
[7] Stix T.H. 1992 *Waves in Plasmas* (New York: AIP)
[8] Hosea J. *et al* 2008 *Phys. Plasmas* **15** 056104 (9pp)
[9] Levinton F.M. *et al* 2007 *Phys. Plasmas* **14** 056119 (9pp)
[10] Jaeger E.F., Berry L.A., D'Azevedo E., Batchelor D.B. and Carter M.D. 2001 *Phys. Plasmas* **8** 1573–83
[11] Brambilla M. 2002 *Plasma Phys. Control. Fusion* **44** 2423–44
[12] Hosea J., Bernabei S., Biewer T., Leblanc B., Phillips C.K., Wilson J.R., Stutman D., Ryan P. and Swain D.W. 2005 *16th Topical Conf. on RF Power in Plasmas* (*Park City, UT, USA*) vol 787 ed S.J. Wukitch and P.T. Bonoli (New York: AIP Conference Proceedings) pp 82–5
[13] Sabbagh S.A. *et al* 2001 *Nucl. Fusion* **41** 1601–12
[14] Nightingale M. 2007 Association Euratom – UKAEA personal communication
[15] Colestock P., Greene G.J., Hosea J.C., Phillips C.K., Stevens J.E., Ono M., Wilson J.R., D'Ippolito D.A., Myra J.R. and Lehrman I.S. 1990 *Fusion Eng. Des.* **12** 43–50
[16] Noterdaeme J.-M. and Van Oost G. 1993 *Plasma Phys. Control. Fusion* **35** 1481–511
[17] Myra J.R., D'Ippolito D.A., Russell D.A., Berry L.A., Jaeger E.F. and Carter M.D. 2005 *16th Topical Conf. on RF Power in Plasmas (Park City, UT, USA)* vol 787 ed S.J. Wukitch and P.T. Bonoli (New York: AIP Conference Proceedings) pp 3–14
[18] Colas L., Faudot E., Brémond S., Heuraux S., Mitteau R., Chantant M., Goniche M, Basiuk V, Bosia G, Gunn J P and the Tore Supra Team 2005 *16th Topical Conf. on RF Power in Plasmas (Park City, UT, USA)* vol 787 ed S.J. Wukitch and P.T. Bonoli (New York: AIP Conference Proceedings) pp 150–7
[19] Gates D. *et al* 2009 Overview of results from the national spherical torus experiment (NSTX) *Nucl. Fusion* at press
[20] Wilgen J.B., Ryan P.M., Hanson G.R. Swain D.W., Bernabei S.I., Greenough N., DePasquale S., Phillips C.K., Hosea J.C. and Wilson J.R. 2006 *Rev. Sci. Instrum.* **77** 10E933 (4pp)
[21] Ehst D.A. and Karney C.F.F. 1991 *Nucl. Fusion 31* 1933–8
[22] Mau T.K. *et al* 2003 *15th Topical Conf. on RF Power in Plasmas (Moran, Wyoming)* vol 694 ed C.B. Forest (New York: AIP Conference Proceedings) pp 205–8
[23] Menard J. 2007 PPPL personal communication
[24] Smirnov A.P., Harvey R.W. and Prater R. 2008 General linear RF-current drive calculations *Proc. EC-15 Conf. on Toroidal Plasma (Yosemite, CA, USA)*
[25] Hawryluk R.J. 1980 *Physics of Plasmas Close to Thermonuclear Conditions* vol 1 ed B. Coppi (Brussels: Commission of the European Communities) pp 19–46
[26] Bonoli P.T. *et al* 2007 *17th Topical Conf. on RF Power in Plasmas (Clearwater, FL, USA)* vol 933 ed P.M. Ryan and D.A. Rasmussen (New York: AIP Conference Proceedings) pp 435–42
[27] LeBlanc B.P. *et al* 2005 *16th Topical Conf. on RF Power in Plasmas Park City, UT, USA* vol 787 ed S.J. Wukitch and P.T. Bonoli (New York: AIP Conference Proceedings) pp 86–9